Minimum Temperatures, Diurnal Temperature Ranges, and Temperature Inversions in Limestone Sinkholes of Different Sizes and Shapes

C. D. WHITEMAN

Pacific Northwest National Laboratory, Richland, Washington

T. HAIDEN

Central Institute for Meteorology and Geodynamics, Vienna, Austria

B. POSPICHAL, S. EISENBACH, AND R. STEINACKER

Department of Meteorology and Geophysics, University of Vienna, Vienna, Austria

(Manuscript received 7 November 2003, in final form 25 February 2004)

ABSTRACT

Air temperature data from five enclosed limestone sinkholes of various sizes and shapes on the Hetzkogel Plateau near Lunz, Austria (1300 m MSL), have been analyzed to determine the effect of sinkhole geometry on temperature minima, diurnal temperature ranges, temperature inversion strengths, and vertical temperature gradients. Data were analyzed for a non-snow-covered October night and for a snow-covered December night when the temperature fell as low as $-28.5°C$. A surprising finding is that temperatures were similar in two sinkholes with very different drainage areas and depths. A three-layer model was used to show that the sky-view factor is the most important topographic parameter controlling cooling for basins in this size range in near-calm, clear-sky conditions and that the cooling slows when net longwave radiation at the floor of the sinkhole is nearly balanced by the ground heat flux.

1. Introduction

A characteristic feature of *karst* topography (a landscape conspicuously influenced by subsurface solution) is small depressions or sinkholes that dimple its surface. Such sinkholes or *dolines* are often found in limestone plateaus or mountain areas where the underlying rocks have been cut by a system of joints that act as underground conduits for water. In the early stages of sinkhole formation (Shelton 1966), the ground sags into shallow sinkholes. Later, as solution progresses, the water is channeled into subterranean passages and the sinkholes may collapse into the larger caverns, forming sinkholes of larger size. In the eastern Alps near Lunz, Austria, an entire mountain plateau (the Hetzkogel Plateau) underlain by limestone at an elevation of about 1300 m MSL contains an array of sinkholes of different sizes. In this area, with a mean annual rainfall of 2200 mm (Sauberer 1947), the sinkholes are well drained and are not filled by lakes. This paper focuses on the cold-air pools (i.e., nighttime temperature inversions) that form regularly in these sinkholes, with the goal of determin-

ing the effects of sinkhole size and geometry on the resultant temperature inversions.

2. Background

A number of previous authors have described measurements of temperature inversions in basins. Basin inversions have been studied in Slovenia (Petkovšek and Rakovec 1983; Vrhovec 1991; Rakovec et al. 2002), Japan (Magono et al. 1982; Maki and Harimaya 1988; Maki et al. 1986; Kondo et al. 1989; Yoshino 1984; Iijima and Shinoda 2000), the western United States (Whiteman et al. 1996; Clements et al. 2003), and in the limestone ranges of the European Alps (Geiger 1965). Most of the basins studied to data have been major basins that contain population centers and where high industrial emissions and persistent inversions cause air pollution problems.

The dolines south of Lunz in a region called the Gstettner-Alm have been previously studied by other investigators, following the reports of extreme minimum temperatures in the largest doline, the Gruenloch basin (Aigner 1952; Schmidt 1930, 1933). Following this early work, Lauscher (1937) investigated the radiation climate of the area, and two tethered-balloon sounding

Corresponding author address: C. David Whiteman, Pacific Northwest National Laboratory, P.O. Box 999, Richland, WA 99352.
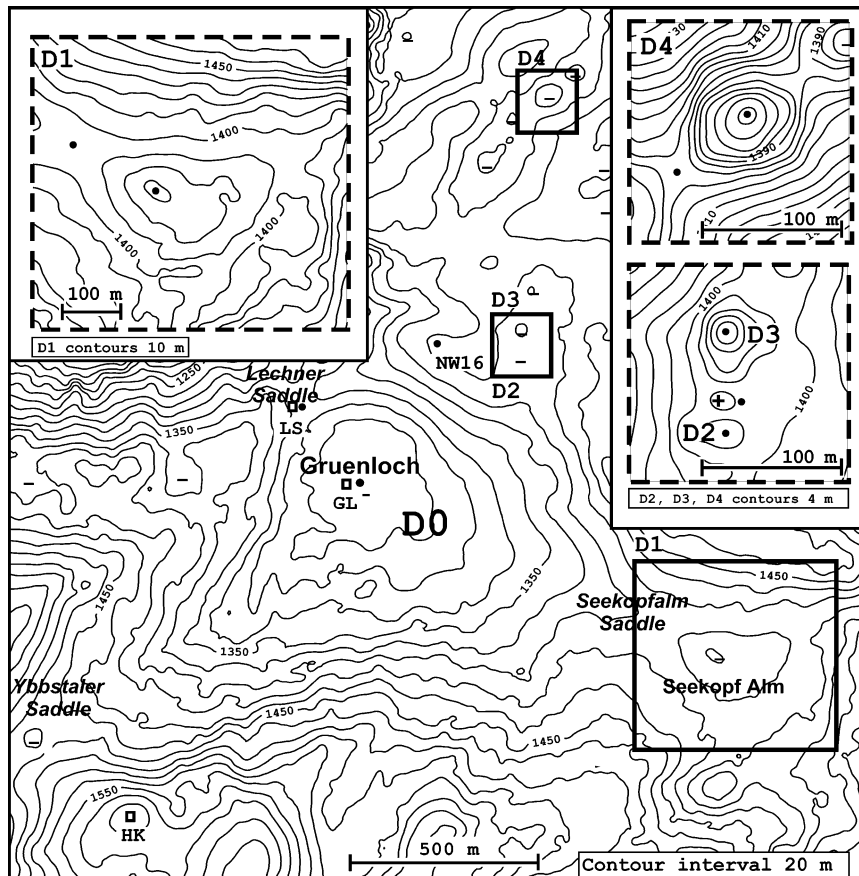E-mail: dave.whiteman@pnl.gov

FIG. 1. Topographic map of the Gruenloch doline (D0) and its surroundings, showing the locations of the saddles, the temperature dataloggers (filled circles), and the automatic weather stations (squares) at the Kleiner Hühnerkogel (HK), the Lechner Saddle (LS), and the Gruenloch (GL). Detailed topographic maps for the areas surrounding dolines D1, D2, D3, and D4 (solid rectangles) are shown as inset figures (dashed rectangles). Note the different length scales and contour intervals in the inset figures. Negative signs on the main map identify the centers of dolines.

campaigns were conducted in the Gruenloch in 1953 and 1954 (Sauberer and Dirmhirn 1954, 1956). The first of these tethered-balloon campaigns, conducted in March with wintertime snow cover, found air temperatures as low as −30.5°C on the basin floor and the development of an impressive 20°C inversion over a depth of 70 m. An unpublished dissertation by Litschauer (1962) investigated many scientific questions on basin climate in Austria and in the Gstettner-Alm in particular, comparing temperature minima and considering the effects of basin size and shape.

In this paper, we compare inversions in sinkholes of different sizes and shapes on selected nights using data from temperature dataloggers that were left in the dolines from October of 2001 through early June of 2002. Another (Whiteman et al. 2004) compares tethersonde temperature profiles over the center of the Gruenloch to pseudovertical temperature soundings obtained from lines of temperature dataloggers that were left on the basin's sidewalls. That comparison gives us confidence that the pseudovertical soundings are useful proxies for free air temperature profiles over the basin center under the stably stratified conditions that are encountered on typical nights.

3. Methods

a. The dolines and the instrument sites

A topographic map of the Gruenloch and its surroundings is shown in Fig. 1. It indicates the relative positions of the individual dolines D0–D4, provides detailed views of the terrain contours around D1–D4, and identifies the measurement sites. Figure 2 shows topographic cross sections through the dolines, and Table 1 summarizes the geometrical characteristics of the dolines. Drainage areas in this table were determined by planimeter from topographic maps; volumes were calculated from the drainage areas by numerical integration. The doline drainage areas and volumes are plotted
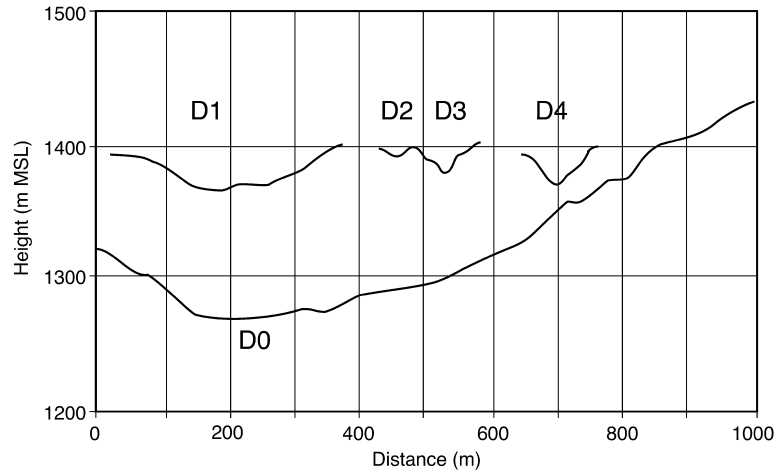
FIG. 2. Topographic cross sections through the five dolines. The origin of the D0 cross section starts at the Lechner Saddle. The other cross sections are plotted at arbitrary distances on the *x* axis but at actual heights on the *y* axis. The sections are made on lines connecting the doline floor and saddle dataloggers and extending through the dolines.

as a function of elevation in Fig. 3. The doline volumes are not well defined above the lowest saddles, because a terrain "opening" is then present. Thus, for elevations above the lowest saddles the volumes are calculated as through there were a vertical wall around the periphery of the doline drainage area. The altitudes of the temperature datalogger and automatic weather station sites and the heights of the temperature sensors are given in Table 2.

b. Meteorological equipment

The measurement equipment and accuracies were described in an overview of the Gruenloch 2001–02 experiments by Steinacker et al. (2002), and so only a brief summary is given here. The primary data are temperature data collected with HOBO H8 Pro temperature dataloggers (Onset Computer, Inc., Bourne, Massachusetts). These dataloggers, which were evaluated for meteorological use by Whiteman et al. (2000), are self-contained, battery-powered devices that use a thermistor sensor having a 2-min time constant. The thermistors were exposed in six-plate nonaspirated radiation shields installed on wooden poles, with instantaneous temperatures recorded at 5-min intervals. Temperature accu-

racy for the dataloggers is $\pm 0.7°C$ over the range from $-40°$ to $+100°C$.

Supplementary measurements were made with three Mobile Automatic Weather Stations (MAWS) 201 (Vaisala, Inc., Helsinki, Finland) located on the Gruenloch floor (GL), on the Lechnergraben Saddle (LS), and on the Kleiner Hühnerkogel (HK), a mountain peak southwest of the Gruenloch. These stations recorded pressure, temperature, relative humidity, wind speed, and wind direction at 5-min averaging intervals. Sensor heights were as follows: pressure—1 m; temperature, humidity, and radiation—1.5 m; and wind speed and direction—2.5 m. Temperature accuracy was 0.3°C over the range from $-40°$ to $+60°C$, relative humidity (RH) accuracy was $\pm 2\%$ for $0 \leq RH \leq 90\%$ and $\pm 3\%$ for $RH \geq 90\%$, wind direction accuracy was less than $\pm 3°$, and wind speed accuracy was 0.3 m s^{-1} for wind speeds below 10 m s^{-1} and less than 2% for winds above 10 m s^{-1}. The wind speed threshold was <1 m s^{-1}, and the distance constant was 2 m. A pyranometer that was used at the Lechnergraben MAWS sites on 18–19 October covered the spectral range from 0.4 to 1.1 μm, with a global radiation accuracy of $\pm 3\%$.

The instruments were operated from 17 October 2001 through 4 June 2002. Because of heavy winter snowfall,

TABLE 1. Topographic characteristics for the five dolines. Sky-view factors are as given by Litschauer (1962) for D0 and D2–D4 and are from a direct measurement for D1. Total drainage areas for D2 and D3 are, to a good approximation, identical.

| Basin	Elev of doline floor (m MSL)	Outflow depth h (m)	Diameter at h (m)	Drainage area A below h (m²)	Volume V below h (m³)	Tot drainage area A_T (m²)	Sky-view factor f_V
D0: Gruenloch	1270	54	600	295 000	7 000 000	2 120 000	0.91
D1: Seekopfalm	1368	26	250	51 000	550 000	245 000	0.88
D2: Unnamed	1393	7	45	1600	2700	313 000	~0.6
D3: Unnamed	1381	19	75	4440	19 300	313 000	~0.6
D4: Unnamed	1372	22	76	4560	41 000	334 500	~0.6
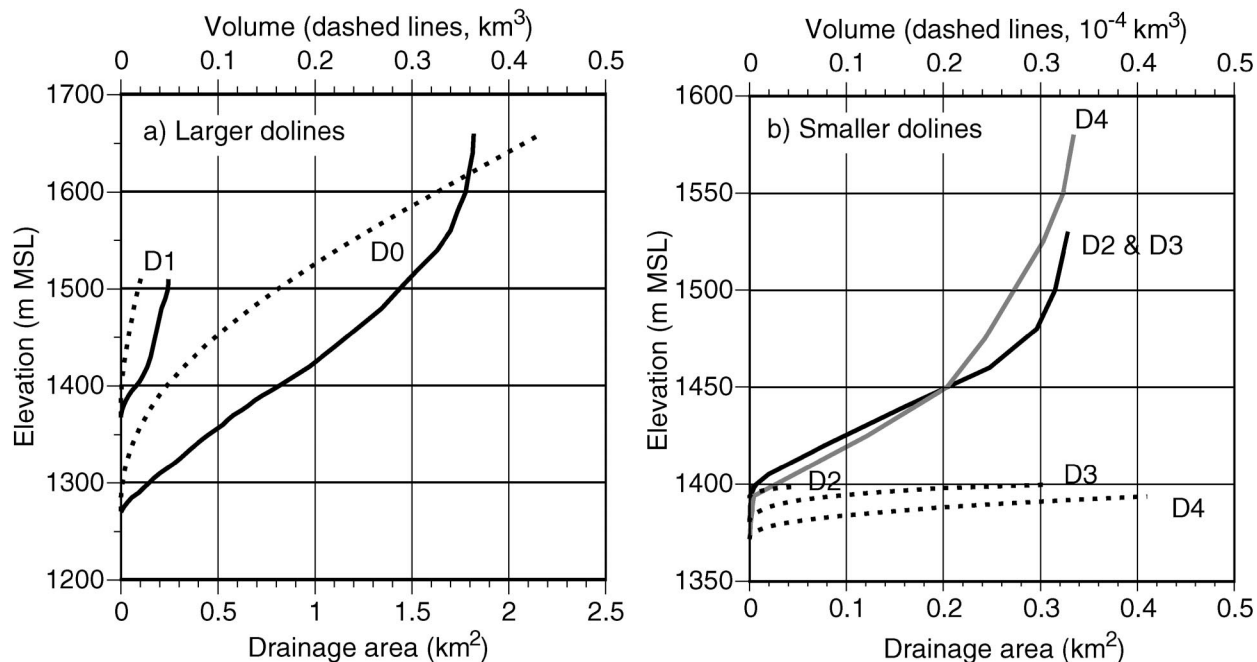
FIG. 3. Drainage area (km², solid line) and volume (km³, dashed line) as a function of height for (a) the two largest dolines and (b) the three smallest dolines.

the solar panels of the weather stations and some of the HOBOs were sometimes beneath the snow cover, causing data interruptions and affecting our choices of case study dates.

c. The experimental design

The research approach was 1) to install temperature dataloggers at the floor and on the lowest saddle of each of the sinkholes, 2) to compare the measured sinkhole temperatures and temperature inversion strengths on clear undisturbed nights, and 3) to use these data to investigate the role of doline geometry on minimum

temperatures, temperature trends, and temperature inversions in the sinkholes.

Instrumenting multiple dolines on the same plateau (as opposed to instrumenting dolines that are tens or hundreds of kilometers apart) ensures that the synoptic conditions will be the same for all dolines. The relative positions of the dolines on the plateau, however, may result in somewhat different exposure to above-plateau winds, and the relatively minor differences in doline saddle elevations exposes them to somewhat different ambient conditions. Further, under certain conditions, fog or stratus might form at different times in the individual dolines. This condition is usually readily apparent in the temperature records.

4. Results

Two clear, undisturbed periods have been chosen for the analyses—one without snow cover (18–19 October 2001) and one with about 0.4 m of snow cover (1–4 December 2001).

a. 18–19 October 2001 (no snow cover)

The Hetzkogel Plateau on this date was affected by a high pressure ridge over central Europe extending from the Mediterranean Sea to Scandinavia. This synoptic situation produced clear skies with weak synoptic-scale winds and no snow cover. Astronomical sunrise occurred at 0629 central European standard time (CEST), astronomical sunset was at 1703 CEST, and

TABLE 2. HOBO and automatic weather station altitudes and temperature sensor heights.

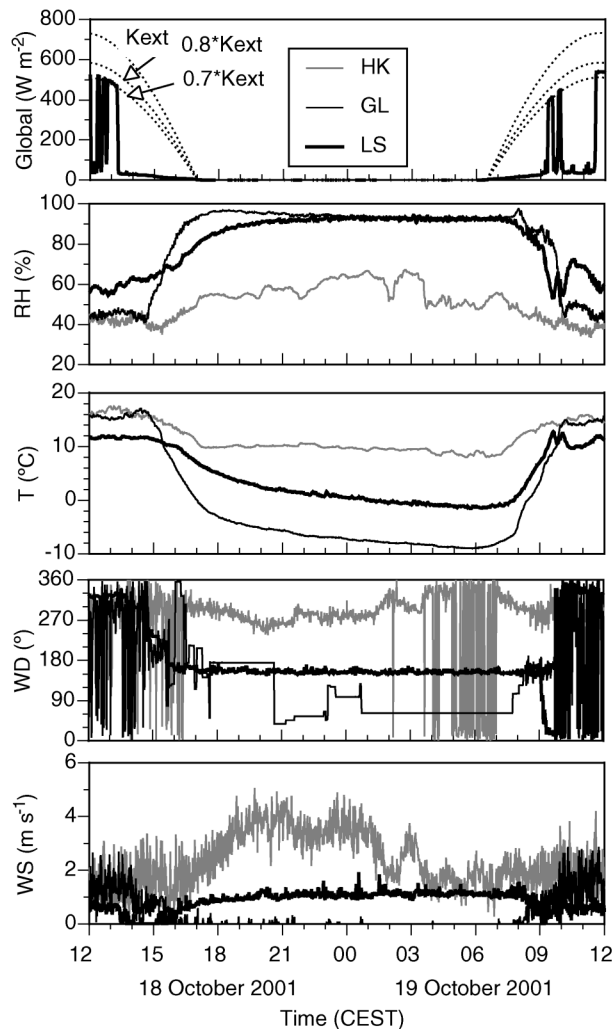| Site	Alt (m MSL)	Height (m AGL)
D0 floor	1270	1.4
D0 saddle	1324	1.4
NW16	1412	1.4
D1 floor	1368	1.4
D1 saddle	1394	1.4
D2 floor	1393	1.4
D2 saddle	1400	1.4
D3 floor	1381	1.4
D3 saddle	1400	1.4
D4 floor	1372	1.4
D4 floor	1372	2.2
D4 saddle	1400	1.4
HK	1601	1.5
LS	1323	1.5
GL	1270	1.5

FIG. 4. Time series of global radiation, relative humidity, temperature, wind direction, and wind speed on 18–19 Oct 2001 at HK, GL, and LS weather stations. Kext is the theoretically determined extraterrestrial solar irradiance.

the theoretical daily total extraterrestrial solar irradiance (19 October) on a horizontal surface was 17.87 MJ m^{-2}.

Local observations from the three weather stations on the plateau (Fig. 4) fit well into the synoptic picture. At the Lechner Saddle, the pyranometer, which was frequently shaded by surrounding trees and topography, recorded about 73% of the instantaneous theoretical or extraterrestrial solar radiation when in the sunlight. The pyranometer, which was in full shadow between 1321 CEST and sunset on 18 October and between sunrise and 0903 CEST on 19 October, recorded a maximum in diffuse solar irradiance at midday of about 40 W m^{-2}. This value is a reasonable estimate of the maximum diffuse radiation on the shaded floors of the nearby sinkholes. Because net outgoing longwave radiation is expected to be greater than this net incoming solar radiation, the floors of the sinkholes will have a negative net radiation balance when in shadow. After about 1430

CEST, a rapid drop in temperature began at the floor of the Gruenloch, accompanied by a rise in relative humidity from 40% to 95%. The rate of temperature decrease slowed appreciably after 1900 CEST. By sunrise, the temperature at the basin floor had dropped by about 25°C. Temperatures dropped by 10°C at the Kleiner Hühnerkogel and 13°C at the saddle. Temperatures at the Kleiner Hühnerkogel remained constant for much of the night, suggesting that there was little horizontal temperature advection in the synoptic-scale environment and that the cooling in the Gruenloch was produced locally.

Winds were variable in direction in the Gruenloch during the early afternoon but often attained the same strength ($\sim$1.5 m s^{-1}) and direction (westerly) as the winds above the doline on the Kleiner Hühnerkogel. The winds became calm after 1530 CEST, when an inversion began to form within the doline. The calm winds continued until 0800 CEST. Between 0800 CEST and noon, the winds gradually increased to 2 m s^{-1} as the atmosphere in the doline gradually became coupled to the synoptic-scale winds aloft, attaining the same speed and direction (northwesterly) as at the Kleiner Hühnerkogel. This coupling occurred during the inversion breakup period when the temperature on the doline floor began its rapid rise. Winds at the saddle gradually increased from near calm (1400–1520 CEST) to a steady nighttime speed of 1 m s^{-1} from the southeast. This late afternoon and nighttime wind represents an overflow of cold air from the doline through the saddle, the topic of a separate research paper by Pospichal et al. (2003). The westerly or northwesterly winds on the Kleiner Hühnerkogel accelerated after 1530 CEST once the temperature inversion began to form in the Gruenloch but died back down to 1.5–2 m s^{-1} by 0400 CEST.

Temperature relationships among the five dolines are shown in Fig. 5. In Figs. 5a and 5b the temperatures at the doline floors and saddles are plotted against time. The floors and saddles attain their lowest temperatures near sunrise. The coldest temperatures occur at the floors of D0 and D1, the dolines with the largest drainage areas, the lowest elevations, and the most topographical relief (Table 1), and the warmest temperatures occur at D2. A surprise is that the temperature traces are nearly identical for D0 and D1, dolines whose drainage areas differ by a factor of 8.6. Also, D3 and D4 have nearly identical nighttime temperature courses. Temperatures on the doline floors can be compared with those at a sidewall site high on the north sidewall of the Gruenloch at NW16 (1412 m MSL) in Fig. 5a. The temperature there fell only 5°C during the night.

The temperature drop from the day's maximum at the doline floor (Fig. 5c) is a measure of the maximum diurnal temperature range within a doline. Diurnal temperature ranges were from 22.3° to 28.1°C at the individual dolines (Table 3). For comparison, the diurnal temperature range at NW16 (1412 m MSL) was 5.9°C (Fig. 5a), and at Kleiner Hühnerkogel (1601 m MSL)
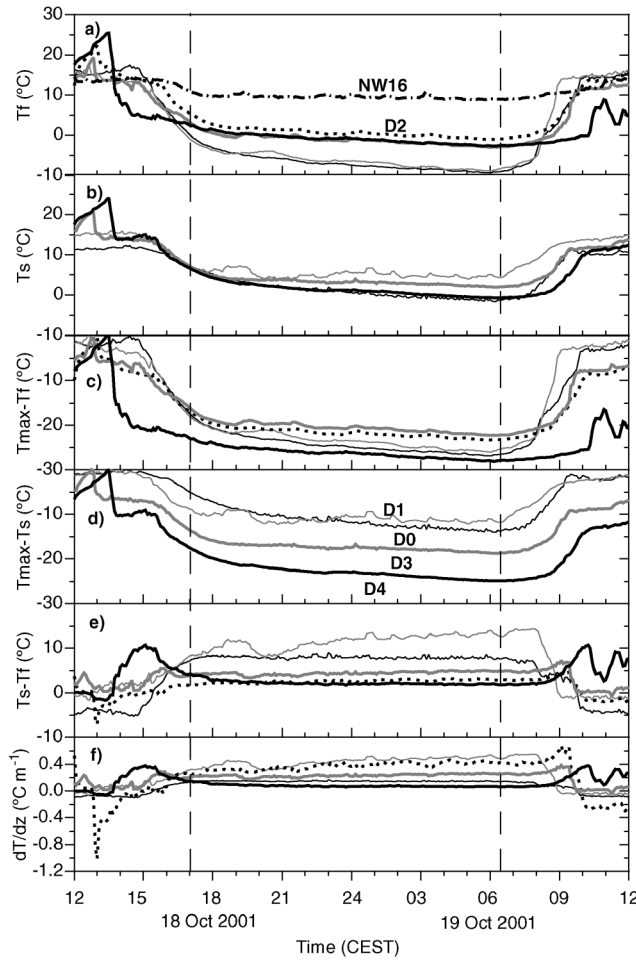
FIG. 5. Temperature relationships among the five dolines (D0–D4) on 18–19 Oct 2001 for (a) temperature at the basin floor Tf, (b) temperature at the lowest saddle Ts, (c) drop in temperature at the basin floor from the daytime maximum, (d) drop in temperature at the basin saddle from the daytime maximum, (e) temperature difference between saddle and floor, Ts − Tf, and (f) temperature gradient (Ts − Tf)/dz, where dz is the height difference between the saddle and the floor of the dolines. NW16, a site above all dolines, is shown for comparison in (a). The vertical dashed lines are the times of astronomical sunrise and sunset. Sites D2 and D3 have identical values in (b) and (d).

it was 9°–10°C (Fig. 4). The doline with the largest diurnal temperature range, D4, experienced a temperature fall of 20.5°C in 65 min, starting at 1330 CEST. This deep, narrow doline fell into shadow earlier in the afternoon than the other dolines. A more gradual cooling began at the other dolines around 1500 CEST at rates from 3° to 7°C h^{-1}. After 1900 CEST, the cooling rates dropped to 0.2°–0.5°C h^{-1}.

In contrast to the fairly narrow range of temperature falls from the local afternoon maxima on the basin floors, the temperature falls at the saddles were variable from doline to doline (Fig. 5d), ranging from 12.1° at D1 to 24.9°C at D4 (Table 3). The temperature difference between the lowest saddles and the doline floors (Fig. 5e) is a measure of the temperature deficit or inversion strength in the doline. At 0600 CEST, the vertical temperature differences ranged from 14.1° at D1 to 2.0°C at D4 (Table 3). Temperature deficits are near constant during the night in all dolines because the rates of cooling at a given time are similar at the doline floor and saddle. The exception is the Seekopfalm (D1), where the doline temperature deficit increases during the night because of a higher cooling rate on the floor than on the saddle. The mean temperature gradients in the dolines, obtained by dividing these temperature differences by the doline depths, are shown in Fig. 5f. The Seekopfalm (D1) had the strongest nighttime vertical temperature gradients. Temperature gradients at 0600 CEST, which are broadly representative of the gradients that were maintained during the night, ranged from 0.54° at D1 to 0.07°C m^{-1} at D4 (Table 3).

It is interesting to note that the maximum temperature deficits and gradients (Figs. 5e and 5f) in all dolines except D0 do not occur at sunrise. Rather, they tend to occur in the hours after sunrise (typically, 0730–1000 CEST) when the shaded doline floors are still cold but the saddles have already started to warm. However, D4 differs from the other dolines in that the maximum temperature deficit and gradient occur in the afternoon at 1500 CEST when the temperature at the floor of the shaded doline has already fallen precipitously but the air above the doline is still warm from the daytime heating over the Hetzkogel Plateau.

TABLE 3. Comparative temperature minima, daily temperature ranges, temperature difference between saddle and basin floor at 0600 CEST, and temperature gradients for the five dolines for 18–19 Oct and 2–3 Dec 2001. Here Tf is temperature at the basin floor, Ts is temperature at the lowest saddle, and dz is height difference.

| Doline	Tf min (°C)		Ts min (°C)		Tf range (°C)		Ts range (°C)		Ts−Tf at 0600 CEST (°C)		(Ts−Tf)/dz at 0600 CEST (°C m^{-1})	
	18–19 Oct	2–3 Dec	18–19 Oct	2–3 Dec	18–19 Oct	2–3 Dec	18–19 Oct	2–3 Dec	18–19 Oct	2–3 Dec	18–19 Oct	2–3 Dec
D0	−9.4	−28.5	−1.6	−13.1	26.9	19.7	14.0	8.5	8.1	15.6	0.15	0.29
D1	−9.0	−27.8	4.0	−10.4	26.0	11.0	12.1	9.4	14.1	20.0	0.54	0.73
D2	−1.0	−16.6	1.9	−9.4	23.3	12.3	18.8	11.0	3.0	7.0	0.43	0.99
D3	−3.0	−21.4	1.9	−9.4	22.3	6.1	18.8	11.0	4.9	11.9	0.26	0.63
D4	−2.7	−24.0	−0.7	−17.5	28.1	5.0	24.9	13.5	2.0	6.5	0.07	0.24
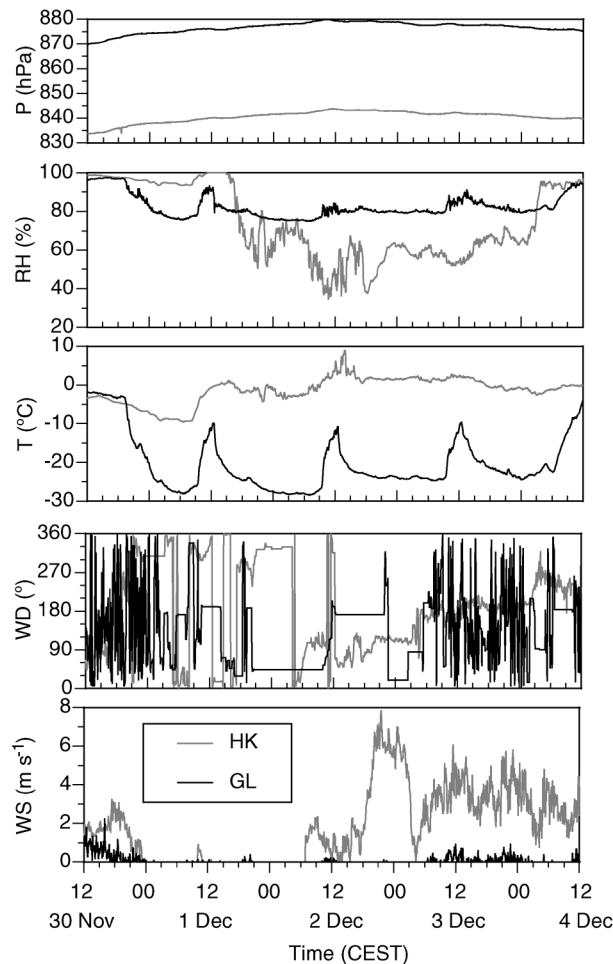
FIG. 6. Time series of pressure, relative humidity, temperature, wind direction, and wind speed on 30 Nov–4 Dec 2001 at the HK and GL weather stations.

b. 1–2 December 2001 (with snow cover)

Although this section will focus on 1–2 December, data from the Kleiner Hühnerkogel and Gruenloch weather stations for 30 November to 4 December 2001 are shown in Fig. 6 to examine the background synoptic conditions and representativeness of this day. On 1 December, astronomical sunrise was at 0734 and sunset was at 1604 CEST; the theoretical daily total extraterrestrial radiation was 9.53 MJ m^{-2} (this is 53% of the 19 October total and 23% of the total at the summer solstice).

A warm-front passage occurred in midday on 30 November, and snowfall, which had occurred over the last 4 days, ended with a total accumulation of about 0.5 m at altitudes corresponding to the Gruenloch. After the frontal passage, a high located over Russia expanded to central Europe, lasting until 4 December. During the 1–4 December period, winds were generally weak and from the north or northeast while temperatures at 850 hPa rose slowly from −2° to +2°C.

Data from the Kleiner Hühnerkogel and Gruenloch automatic weather stations (Fig. 6) showed how the local conditions changed with the evolving synoptic situation. The pressure rose and the skies cleared after the frontal passage. Freezing of the new wet snow on the wind vanes and anemometers at HK and GL degraded the wind data off and on for the following 2 days.

Humidity was over 90% at both HK and GL at noon on 30 November but fell at GL starting in the evening, and it remained near constant at 80% until 4 December, except for an excursion to 90% in late morning on 1 December. At HK, humidity exceeded 90% until midafternoon on 1 December, when it dropped to 60% and oscillated between 40% and 80% until midnight on 4 December when it rose again to values above 90%.

Temperatures fell at HK and GL during the afternoon and night of 30 November. After the morning temperature rise on 1 December, the temperature at HK remained mostly steady for the next 3 days. The temperature at the floor of the Gruenloch, on the other hand, underwent strong diurnal oscillations indicating buildup and decay of nocturnal inversions, with nighttime temperatures falling at sunrise to quasi-equilibrium values as low as −27°C, daytime temperatures rising to −10°C, and sharp rises and falls occurring in late morning and early afternoon in response to the doline's solar illumination and shadowing. Despite the strong midday warming on the basin floor, the Gruenloch cold-air pool was maintained continuously during the 1–4 December period [inversion destruction would require that the temperature difference between HK and GL be $\Delta T \leq \Gamma_d \Delta z = 0.0098 \times (1601 - 1270) = 3.2°C$, where Γ_d is the dry adiabatic lapse rate and Δz is the height difference between the two sites]. Winds were calm at GL within this persistent cold-air pool. Winds at HK were from the northwest or north until about 0400 CEST on 2 December when, over a 24–30-h period, they veered slowly into the northwest. Speeds at HK were generally below 4–5 m s^{-1} during the 30 November–4 December period except during the middle of the night on 2–3 December.

Temperature time series for sites on the floors of the five dolines (D0–D4) and for a site located on a sidewall of the Gruenloch above the dolines (NW16) are shown in Fig. 7. Because the lower (1.4 m AGL) HOBO at D4 was covered by snow, we use data from the upper (2.2 m AGL) HOBO in this analysis. The time series shows a regular, repeatable behavior in the relative sinkhole temperatures from day to day following the snowfall on 30 November, except for a general warming trend and nighttime disturbances in the cooling at all doline floor sites during the nights of 2–3 and 3–4 December. At D2, cooling disturbances were present on all nights. Subsequent analyses will focus on the night of 1–2 December, when winds aloft were light (≤2 m s^{-1}) and temperatures in the doline underwent a diurnal oscillation representative of a quiescent night following fresh snow.
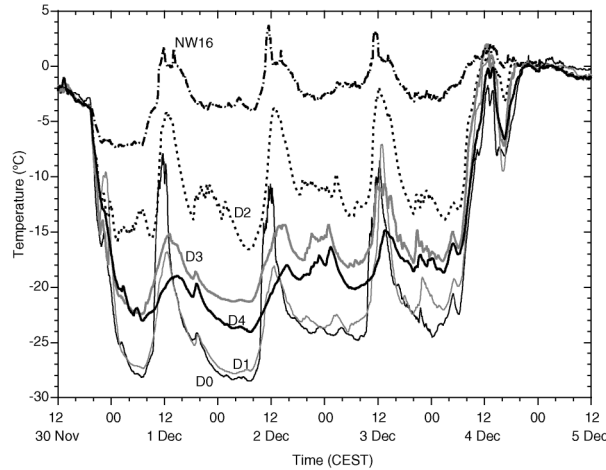
FIG. 7. Multiday temperature time series for sites on the floors of the five dolines and for a site located above the dolines (NW16), 30 Nov–5 Dec 2001. The HOBO at 2.2 m AGL is used at D4; other HOBOs are at 1.4 m AGL.

Temperatures for the dolines are plotted in Fig. 8 in a form parallel to Fig. 5 to facilitate comparisons between the non-snow-covered autumn case and the snow-covered winter case. Three key differences are apparent—1) temperatures were much colder in the winter case and, because of the longer night, lower sun angles, and higher albedos, 2) the diurnal oscillations were suppressed, leading to 3) persistent multiday cold pools in the dolines. Figure 8a shows that, as in the October case, D0 and D1 experienced very similar temperatures despite the very different physical characteristics of the dolines, with the temperatures falling to −28.5°C on the floor of the Gruenloch and −27.8°C on the floor of the Seekopfalm (Table 3). Like the October case, temperatures on the doline floors increase from D0 to D1 to D4 to D3 to D2 and to NW16. The strongest diurnal warming–cooling cycle occurred in the Gruenloch, the only doline with forests on its sidewalls; other dolines have their sidewalls covered with high-albedo snow. Cold pools persisted in the dolines all day, as indicated by the markedly different floor temperatures in midday (in a well-mixed dry adiabatic atmosphere, the temperature differences among dolines D1–D4 would be less than 0.25°C, because they differ in altitude by only 25 m). Temperatures at the lowest saddles above each of the dolines (Fig. 8b) underwent about the same 15°C diurnal oscillation as in October, and the relative temperatures of the doline saddles were also similar (Table 3). Midday temperature rises were larger at the saddles than at the doline floors because the saddles were not in shade as long as the doline floors and because heating of the upper elevations of the basin was facilitated by the forests there.

The decreases in doline floor temperatures from the daytime maxima (Fig. 8c) differed from those seen in October (Table 3). Most notable was the small 5.0°C drop at D4, the site with the largest October drop

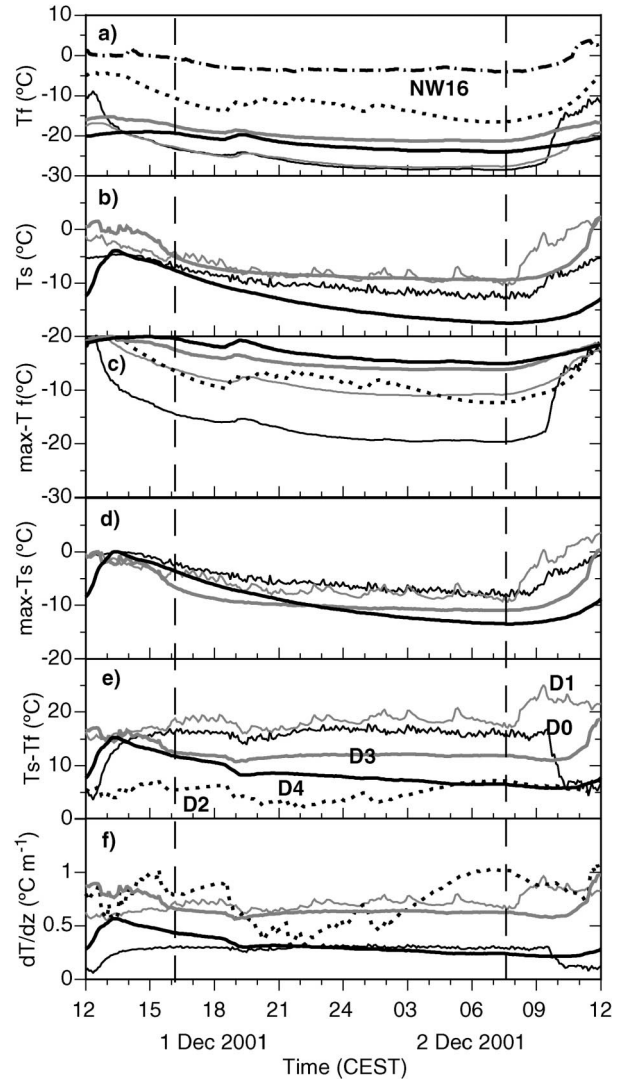FIG. 8. Same as Fig. 4, but for 1–2 Dec 2001.

(20.5°C). This site was already very cold at midday and, in midwinter, experiences little daytime warming because it is in shadow. Diurnal temperature ranges were from 19.7° at D0 to 5.0°C at D4 (Table 3). Diurnal temperature ranges at the saddles (Fig. 8d) were from 13.5° at D4 to 8.5°C at D0. At D4 and D5, the diurnal temperature ranges at the saddles were larger than at the basin floors. Differences in temperature between the saddles and floors of the dolines (i.e., the inversion strengths; Fig. 8e) were larger in December than in October, with no negative values—again emphasizing that the winter cold pools were multiday pools that were not destroyed by midday heating (Table 3). Nighttime inversion strengths differed from doline to doline as in October, although they were not as steady during the night as in October. At 0600 CEST, the values ranged from 20.0° at D1 to 6.5°C at D4. The temperature gradients in the individual dolines (Fig. 8f), as in October,

remained steady throughout the night (except at D2). The temperature gradients in the dolines were, however, considerably stronger in December than in October. At 0600 CEST, they ranged from 0.99° at D2 to 0.24°C m^{-1} at D4.

5. Discussion

The fact that the sinkholes D0 and D1, despite their different sizes, depths, and drainage areas, experience very similar nighttime temperatures is a significant finding that forces us to revisit the theory of nighttime cooling in closed basins. Whereas temperatures at D0 and D1 differ markedly during daytime (because of different local sunrise and sunset times, different degrees of inversion breakup, etc.) they approach each other soon after local sunset and remain within ~1°C throughout the night. Any head start of D1 as compared with D0 in terms of cooling (Figs. 5 and 8) is rapidly lost early in the night. The short time constant of the process suggests the presence of a strong negative feedback of temperature on the cooling process. This suggestion is confirmed by the behavior of the temperature curves after other intermittent disturbances (not shown). After such episodes, D1, which is more susceptible to the ambient wind, manages to catch up quickly with the temperature trace at D0.

Let us consider limiting cases. The temperature at the bottom of a sinkhole could be the result of a cooling process that is (almost) independent of temperature. Then intermittent warming episodes would not be energetically "forgotten," leading to a permanent cooling lag in the system. In the other extreme, the temperature could be the result of a quasi equilibrium between cooling and (almost) equal opposing warming processes, in which any temperature change initiates strong counteracting mechanisms. In such a system the temperature would quickly recover once ambient wind effects cease. Observational evidence suggests that during most of the night the air near the bottom of the sinkhole is close to the strong-feedback, quasi-equilibrium state. Below, we present a highly simplified model of near-surface cooling to analyze this quasi equilibrium theoretically.

Over flat terrain under undisturbed conditions with weak synoptic flow, nighttime cooling of near-surface air is primarily caused by net longwave radiative loss from the uppermost soil layer (and vegetation, if present). Radiative cooling of the soil at the soil–air interface produces a downward sensible heat flux from the adjacent air, which acts as a negative feedback to counteract the cooling of the soil. Once the uppermost soil layer has cooled sufficiently, an upward sensible heat flux from warmer, deeper layers will begin to counteract surface cooling as well. A third negative feedback is associated with the longwave radiative flux itself. The more the surface cools relative to the air at higher levels, the smaller the net outgoing radiation will be. As a result of the negative feedbacks, near-surface temperature decreases more and more slowly during the course of a night.

In what way is the cooling process in a closed basin different from the process over flat terrain? The concave shape of the topography keeps the air close to the basin floor from being mixed by the ambient flow once a stable stratification has developed. Thus, at the basin floor windless conditions will be established earlier in the night and maintained more easily against any shear-induced turbulence that may be intermittently generated at higher levels even in weak flow situations. Once the temperature near the basin floor has become several degrees colder than the air at the basin rim, there will be very little direct advection of air from the rim all the way down to the basin floor. By cooling down fastest (because it does not move), the air at the basin floor quickly isolates itself from air at higher levels. Thus, while katabatic flows may still drain toward the basin, they do not directly lead to air exchange near the basin floor but enter the basin atmosphere at higher levels. The lack of mass exchange between the sinkhole floor and the slopes could explain why D0 and D1, despite their different topographic characteristics, show extremely similar temperature traces even during the initial, rapid cooling phase.

Another consequence of concave topography is the reduced view of the sky. It means that part of the downward longwave radiation at the basin floor does not originate in the atmosphere, but from surrounding terrain. This effect can be expressed in the form of a sky-view factor $f_V = \cos^2\alpha$, where α is the average elevation angle of the horizon (Marks and Dozier 1979). The downward longwave radiation flux density assumes the form

$$L^\downarrow = f_V \varepsilon_A \sigma T_A^4 + (1 - f_V)\varepsilon_S \sigma T_S^4, \qquad (1)$$

where ε denotes emissivity, σ is the Stefan–Boltzmann constant, and the subscripts A and S denote the atmosphere and surface, respectively. Table 1 shows that the two coldest dolines D0 and D1 have sky-view factors close to 0.9, whereas the smaller dolines are estimated to have values around 0.6. In all cases, the effect of forest surrounding the basins was taken into account in the determination of the sky-view factor (Litschauer 1962).

Equation (1) is strictly valid only if the surface temperature T_S is uniform. In the case of basin cooling we must take into account the fact that the basin wall temperature T_W will be different from, and on average higher than, the basin floor surface temperature T_S. This difference leads to a stronger increase of incoming radiation than predicted by (1). Within the framework of simple analytical modeling, an improved estimation of reduced sky-view effects can be derived as follows. The upward longwave flux is given by

$$L^\uparrow = \varepsilon_S \sigma T_S^4, \qquad (2)$$

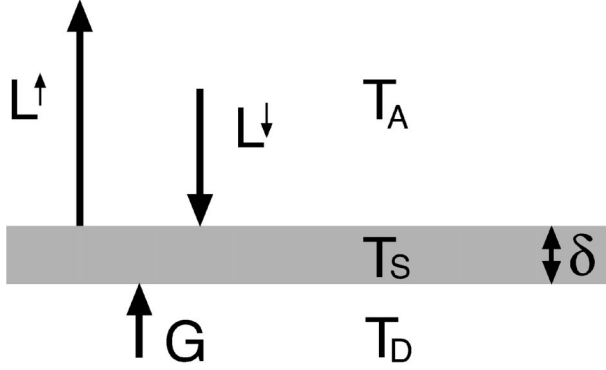as over flat terrain. The downward longwave flux at the

FIG. 9. Idealized three-layer model of surface cooling corresponding to (4). The surface soil layer at a temperature T_S loses heat by longwave radiation exchange with the atmosphere at an effective radiation temperature T_A and gains heat by conduction from a deeper layer at a temperature T_D.

basin floor consists of a contribution from the atmosphere and a contribution from the basin sidewalls:

$$L^\downarrow = f_v \sigma \varepsilon_A T_A^4 + (1 - f_v)\sigma \varepsilon_S T_W^4, \qquad (3)$$

where the sidewall temperature T_W will be somewhere in between the basin floor temperature T_S and the rim temperature T_A. This condition can be expressed in the form $T_W = (1 - g)T_S + gT_A$, where g is a parameter that depends on the geometry of the basin. Combining (2), (3), and the expression for T_W gives for the net outgoing longwave radiation:

$$L_{NET} = L^\uparrow - L^\downarrow = f_v \sigma(\varepsilon_S T_S^4 - \varepsilon_A T_A^4)$$
$$+ g(1 - f_v)\sigma \varepsilon_S(T_S^4 - T_A^4). \qquad (4)$$

The second term on the right-hand side of (4) is zero if the sidewall temperature is identical to the floor temperature ($g = 0$). In this case (4) reduces to the standard expression presented in the literature (Marks and Dozier 1979).

Under windless conditions the sensible heat flux from the atmosphere to the ground will be small (Clements et al. 2003), ultimately approaching the molecular flux value. Thus, downward longwave radiation and upward sensible heat flux from deeper soil layers remain the only processes to counteract longwave cooling of the soil surface. This process is illustrated schematically in Fig. 9 where a surface soil layer with thickness δ loses heat by longwave emission and receives heat from two reservoirs at constant, or slowly varying, temperatures T_A and T_D. A simplified prognostic equation for the time evolution of soil surface temperature can be written in the form

$$\delta c_S \rho_S \frac{dT_S}{dt} = -L_{NET} + G = f_v \sigma(\varepsilon_A T_A^4 - \varepsilon_S T_S^4)$$
$$+ g(1 - f_v)\sigma \varepsilon_S(T_A^4 - T_S^4)$$
$$+ \frac{\nu_S}{D}(T_D - T_S), \qquad (5)$$

where c_S, ν_S, and ρ_S are the specific heat capacity, thermal conductivity, and density of the surface soil layer, respectively. The length scale D represents the effective depth over which the temperature difference $T_D - T_S$ extends. Equation (4) is highly idealized because it reduces the heat exchange at the interface of two continuous media to a three-layer problem. Models employing this type of formulation for the soil heat flux are also known as "force–restore" models. They have been used in global circulation (see, e.g., Bhumralkar 1975) and boundary layer (Stull 1988) modeling and represent an approximation to the vertical diffusion equation equivalent to considering only the leading sinusoidal mode of the forcing (Dickinson 1988). For our problem, the approach provides the simplest possible way of representing the cooling process with the feedbacks envisaged above. If we define as an initial condition $T_S(t = 0) = T_{S0}$ and linearize (5) by replacing T_S^4 with $T_{S0}^4 + 4T_{S0}^3(T_S - T_{S0})$, we obtain, after some reordering of terms, the equation

$$\delta c_S \rho_S \frac{dT_S}{dt} = AT_A^4 + 3BT_{S0}^4 + \frac{\nu_S}{D}T_D - \left(4BT_{S0}^3 + \frac{\nu_S}{D}\right)T_S, \qquad (6)$$

where $A = f_v \sigma \varepsilon_A - g(1 - f_v)\sigma \varepsilon_S$ and $B = f_v \sigma \varepsilon_S - g(1 - f_v)\sigma \varepsilon_S$. Equation (6) is of the form $dT_S/dt = a - bT_S$, giving a negative-exponential solution for the soil surface temperature as a function of time:

$$T_S(t) = T_{S0}e^{-t/\tau} + T_{S\infty}(1 - e^{-t/\tau}), \qquad (7)$$

where

$$\tau = \frac{\delta c_S \rho_S}{4BT_{S0}^3 + \dfrac{\nu_S}{D}} \quad \text{and}$$

$$T_{S\infty} = \frac{AT_A^4 + 3BT_{S0}^4 + \dfrac{\nu_S}{D}T_D}{4BT_{S0}^3 + \dfrac{\nu_S}{D}}.$$

The temperature in the surface soil layer asymptotically approaches the equilibrium temperature $T_{S\infty}$, which is a function of the temperatures of the two reservoirs. Once the temperature gets close to the equilibrium value, net longwave radiation is nearly balanced by the ground heat flux, and further cooling of the surface is small. The time constant of the approach is largely determined by, and is sensitive to, soil parameters.

Using the parameter values listed in Table 4, we have evaluated (7) for the sky-view factors 0.9, and 0.6 corresponding to sinkholes D0–D1, and D2–D4, respectively. The reservoir temperatures were set equal to the temperature of the surface at the beginning of the cooling process. Atmospheric emissivity was set to a typical value of 0.7 (Holtslag and de Bruin 1988).

The resulting net outgoing longwave flux assumed

TABLE 4. Parameter values used to compute the idealized cooling curves shown in Fig. 10. Soil parameters were chosen following Pielke (1984), and with atmospheric emissivity according to Holtslag and de Bruin (1988).

Parameter	Value	Comment
$T_A = T_{S0}$	288.15 K	Corresponding to observed temperature at the beginning of cooling
T_D	278.15 K	Tuned to approximately match equilibrium T_∞ temperature
ϵ_A	0.7	Typical clear-sky atmospheric emissivity
ϵ_S	0.95	Average for mixture of grass and limestone gravel
δ	0.02 m	Tuned to match rapid initial cooling
D	0.5 m	Typical penetration depth of surface cooling
ρ_S	1500 kg m^{-3}	Average for mixture of light soil and rock
c_s	1000 J kg^{-1} K^{-1}	Average for mixture of light soil and rock
ν_S	1 W m^{-1} K^{-1}	Average for mixture of light soil and rock

realistic values of about 80 W m^{-2} at the beginning and strongly decreased to values on the order of 10–20 W m^{-2} later in the night. A small thickness on the order of 2 cm (cf. Table 4) has to be assumed for the thermally active surface soil layer to obtain the rapid temperature drop during the first hours of the cooling. The sidewall temperature parameter had to be set to $g = 0.8$, corresponding to sidewalls significantly closer to basin rim temperature than to basin floor temperature. Figure 10 shows a comparison of modeled surface temperatures and observed temperatures at 1.5-m height. We assume that even during calm conditions the temperature at 1.5-m height evolves largely parallel to the surface temperature. The model reproduces the basic characteristics of the observed cooling curves, in particular their dependence on the sky-view factor. This result suggests that the sky-view factor is indeed the most important topographic parameter controlling basin cooling. Additional evidence for this hypothesis is provided by Litschauer (1962), who noted that the "Untere Legstein-

alm" sinkhole (not studied here) reportedly experiences temperatures almost as low as the Gruenloch (D0), even though it has a much lower saddle. Its sky-view factor is 0.88 (Litschauer 1962), and thus it is very similar to D0 and D1.

The dominant influence of the sky-view factor or aspect ratio on the cooling and the near independence from other topographic parameters such as absolute size and depth obviously cannot carry over to ever smaller basins. We do not observe inversions as strong as those reported here (20–30 K) in depressions of, say, 1-m depths. As the basin gets shallower, complete protection from shear-induced turbulence will no longer occur. Even in cases in which ambient winds were so weak that a completely calm state could be attained, however, vertical temperature gradients would be limited by direct radiative heat exchange within the air. Furthermore, only in a sufficiently deep basin can cooling of the bulk of the basin atmosphere lead to a significant reduction of downward longwave radiation at the basin floor. During the course of the night the surface at the floor of a deep sinkhole radiatively "sees" an increasingly colder atmosphere. This fact could explain why the observed temperature curves in Fig. 10 do not approach a constant equilibrium temperature as in the idealized model, but keep dropping at a low rate throughout the night. The slow cooling during the second half of the night would then merely be the result of slowly decreasing T_A. Observational evidence for this hypothesis has been presented by Eisenbach et al. (2003). Their Fig. 2 shows that during the second half of the night the temperatures at the basin floor and at the height of the lowest saddle (50 m above the floor) decrease at the same rate. This "basin atmosphere" effect would be weak or absent in very shallow basins.

The expression derived for the equilibrium temperature can be used to explain observations of extreme sinkhole temperature minima and intense inversion buildup that occur after fresh snowfalls. Record temperature minima in sinkholes and basins generally occur on clear, windless nights following a fresh fall of new snow (Geiger 1965). The snow cover provides an insulating layer that reduces the upward ground heat flux that normally counters longwave radiation loss from the
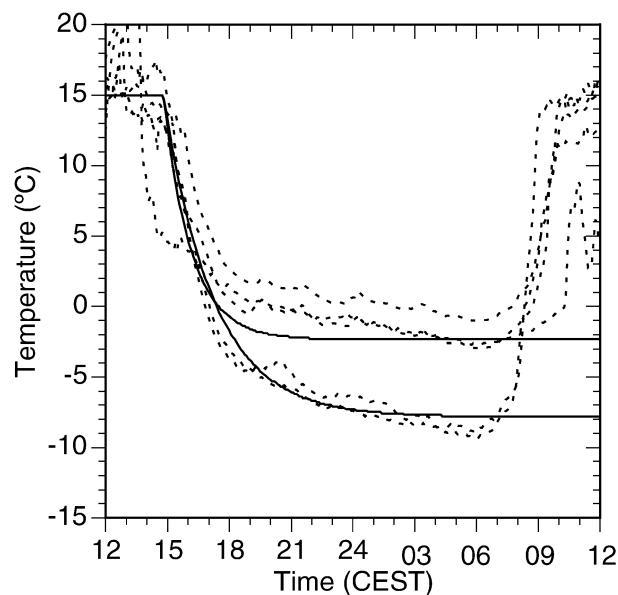

FIG. 10. Comparison of the observed temperature evolution in sinkholes D0–D4 (dashed lines) with results of the idealized model (solid lines) for sky-view factors of 0.9 (lower curve) and 0.6 (upper curve).

surface. The outgoing longwave flux from a fresh snow surface, in contrast, differs little from that of soil at the same temperature, because the emissivities are comparable. With smaller thermal conductivity, the equilibrium temperature in a shallow layer at the upper surface of the snowpack is thus reduced from the case with no snow cover.

6. Conclusions

Limestone sinkholes or dolines of different sizes and shapes are found at an altitude near 1300 m MSL on a mountain plateau near Lunz, Austria. The floors and lowest saddles of five dolines varying in diameter from 45 to 600 m and in depth (floor to lowest saddle) from 7 to 54 m were instrumented with temperature dataloggers to investigate the dependence of temperature minima, diurnal temperature range, temperature inversion strength, and vertical temperature gradient on doline geometry and snow cover. Inversions underwent complete buildup–destruction cycles on a non-snow-covered October day but persisted for multiple days during a snow-covered December period. Temperature minima were lowest in the deepest sinkhole, falling to $-9.4°C$ on the October day and to $-28.5°C$ on the December day. A surprise was that temperatures fell to nearly these same levels in a 26-m-deep sinkhole that had only 12% of the drainage area of the larger sinkhole. Daily temperature ranges at the sinkhole floors were much larger in October than in December, reaching a maximum of $28.1°C$ in the 26-m-deep sinkhole. Inversion strengths and vertical temperature gradients were stronger in December than in October and were strongest in a 7-m-deep sinkhole and a 26-m-deep sinkhole. Nighttime vertical temperature gradients reached nearly $1°C\ m^{-1}$. Gradients were even stronger in some sinkholes during winter mornings after sunrise when temperatures at the saddles warmed up faster than at the still-shaded basin floors.

The observed close correspondence of basin floor cooling in two sinkholes of different sizes but with similar aspect ratios suggests that the sky-view factor is the single most important topographic parameter determining minimum temperatures in sinkholes of different geometry during calm, clear-sky conditions. An idealized three-layer model, in which we have extended the sky-view factor concept to account for radiation from sidewalls that have a temperature intermediate between the basin floor and in the above-basin atmosphere, is used to illustrate the main physical concepts. After a rapid initial cooling phase, a near equilibrium is established between net longwave radiative loss at the surface and the upward flux of heat from the ground. The model also provides a physical explanation for the extreme temperature minima that occur on clear, windless nights following a fresh snowfall.

REFERENCES

Aigner, S., 1952: Die Temperaturminima im Gstettnerboden bei Lunz am See, Niederösterreich (The minimum temperatures in the Gstettner basin near Lunz, Lower Austria). *Wetter Leben,* Special Issue, 34–37.

Bhumralkar, C. M., 1975: Numerical experiments on the computation of ground surface temperature in an atmospheric general circulation model. *J. Appl. Meteor.,* **14,** 1246–1258.

Clements, C. B., C. D. Whiteman, and J. D. Horel, 2003: Cold-air-pool structure and evolution in a mountain basin: Peter Sinks, Utah. *J. Appl. Meteor.,* **42,** 752–768.

Dickinson, R. E., 1988: The force–restore model for surface temperatures and its generalizations. *J. Climate,* **1,** 1086–1097.

Eisenbach, S., B. Pospichal, C. D. Whiteman, R. Steinacker, and M. Dorninger, 2003: Classification of cold air pool events in the Gstettneralm, a sinkhole in the Eastern Alps. *Extended Abstracts, Int. Conf. on Alpine Meteorology and MAP-Meeting,* Brig, Switzerland, MeteoSwiss, Publication 66, 157–160. [Available from MeteoSwiss, Krähbülstrasce 58, Postfach 514, Ch-8044, Zurich, Switzerland.]

Geiger, R., 1965: *The Climate Near the Ground.* Harvard University Press, 482 pp.

Holtslag, A. A. M., and H. A. R. de Bruin, 1988: Applied modeling of the nighttime surface energy balance over land. *J. Appl. Meteor.,* **27,** 689–704.

Iijima, Y., and M. Shinoda, 2000: Seasonal changes in the cold-air pool formation in a subalpine hollow, central Japan. *Int. J. Climatol.,* **20,** 1471–1483.

Kondo, J., T. Kuwagata, and S. Haginoya, 1989: Heat budget analysis of nocturnal cooling and daytime heating in a basin. *J. Atmos. Sci.,* **46,** 2917–2933.

Lauscher, F., 1937: Grundlagen des Strahlungsklimas der Lunzer Kleinklimastationen (Fundamentals of the radiation climate of the Lunz microclimate stations). Jahrbuch der Zentralanstalt für Meteorologie u. Geodynamik (Vienna), Suppl. 4, 1–24.

Litschauer, D., 1962: Untersuchung der Entwicklung von Kaltluftseen

in Dolinen- und Beckenlagen (Investigation of the development of cool air pools in sinkholes and basins). Ph.D. dissertation, University of Vienna, 129 pp.

Magono, C., C. Nakamura, and Y. Yoshida, 1982: Nocturnal cooling of the Moshiri Basin, Hokkaido in midwinter. *J. Meteor. Soc. Japan,* **60,** 1106–1116.

Maki, M., and T. Harimaya, 1988: The effect of advection and accumulation of downslope cold air on nocturnal cooling in basins. *J. Meteor. Soc. Japan,* **66,** 581–597.

——, ——, and K. Kikuchi, 1986: Heat budget studies on nocturnal cooling in a basin. *J. Meteor. Soc. Japan,* **64,** 727–740.

Marks, D., and J. Dozier, 1979: A clear-sky longwave radiation model for remote alpine areas. *Arch. Meteor. Geophys. Bioklimatol.,* **B27,** 159–187.

Petkovšek, Z., and J. Rakovec, 1983: Modeling of cool pool dissipation. *Razprave—Papers (Ljubljana),* **27,** 53–63.

Pielke, R. A., 1984: *Mesoscale Meteorological Modeling.* Academic Press, 612 pp.

Pospichal, B., S. Eisenbach, C. D. Whiteman, R. Steinacker, and M. Dorninger, 2003: Observations of the cold air outflow from a basin cold pool through a low pass. *Extended Abstracts, Int. Conf. on Alpine Meteorology and MAP-Meeting,* Brig, Switzerland, MeteoSwiss, Publication 66, 153–156. [Available from MeteoSwiss, Krähbülstrasse 58, Postfach 514, CH-8044, Zurich, Switzerland.]

Rakovec, J., J. Merše, S. Jernej, and B. Paradiž, 2002: Turbulent dissipation of the cold-air pool in a basin: Comparison of observed and simulated development. *Meteor. Atmos. Phys.,* **79,** 195–213.

Sauberer, F., 1947: Kleinklimatische Niederschlagsuntersuchungen im Lunzer Gebiet (Microclimatic precipitation investigations in the Lunz area). *Die Umwelt,* **2,** 410–415.

——, and I. Dirmhirn, 1954: Über die Entstehung der extremen Temperaturminima in der Doline Gstettner-Alm (On the occurrence of extreme temperature minimums in the Gstettner-Alm Doline). *Arch. Meteor. Geophys. Bioklimatol.,* **5B,** 307–326.

——, and ——, 1956: Weitere Untersuchungen über die Kaltluftansammlungen in der Doline Gstettner-Alm bei Lunz im Niederösterreich (Further investigations of the cold air buildup in the Gstettner-Alm doline near Lunz in lower Austria). *Wetter Leben,* **8,** 187–196.

Schmidt, W., 1930: Die tiefsten Minimumtemperaturen in Mitteleuropa (The lowest minimum temperatures in central Europe). *Die Naturwissenschaften,* **18,** 367–369.

——, 1933: Kleinklimatische Beobachtungen in Österreich (Microclimatic observations in Austria). *Geogr. Jahresbericht Österreich,* **16,** 53–59.

Shelton, J. S., 1966: *Geology Illustrated.* W. H. Freeman, 434 pp.

Steinacker, R., M. Dorninger, S. Eisenbach, A. M. Holzer, B. Pospichal, C. D. Whiteman, and E. Mursch-Radlgruber, 2002: A sinkhole field experiment in the eastern Alps. Preprints, *10th Conf. on Mountain Meteorology,* Park City, UT, Amer. Meteor. Soc., 91–92.

Stull, R. B., 1988: *An Introduction to Boundary Layer Meteorology.* Kluwer, 670 pp.

Vrhovec, T., 1991: A cold air lake formation in a basin—A simulation with a mesoscale numerical model. *Meteor. Atmos. Phys.,* **46,** 91–99.

Whiteman, C. D., T. B. McKee, and J. C. Doran, 1996: Boundary layer evolution within a canyonland basin. Part I: Mass, heat, and moisture budgets from observations. *J. Appl. Meteor.,* **35,** 2145–2161.

——, J. M. Hubbe, and W. J. Shaw, 2000: Evaluation of an inexpensive temperature datalogger for meteorological applications. *J. Atmos. Oceanic Technol.,* **17,** 77–81.

——, S. Eisenbach, B. Pospichal, and R. Steinacker, 2004: Comparison of vertical soundings and sidewall air temperature measurements in a small Alpine basin. *J. Appl. Meteor.,* in press.

Yoshino, M. M., 1984: Thermal belt and cold air drainage on the mountain slope and cold air lake in the basin at quiet, clear night. *GeoJournal,* **8.3,** 235–250.